 Related Commentary, page 2391

Aberrant activation of integrin $\alpha_4\beta_7$ suppresses lymphocyte migration to the gut

Eun Jeong Park,[1,2] J. Rodrigo Mora,[1,3,4] Christopher V. Carman,[5] JianFeng Chen,[1,3] Yoshiteru Sasaki,[1,3] Guiying Cheng,[1,3] Ulrich H. von Andrian,[1,3] and Motomu Shimaoka[1,2]

[1]CBR Institute for Biomedical Research, Boston, Massachusetts, USA. [2]Department of Anesthesia, [3]Department of Pathology, [4]Gastrointestinal Unit, Massachusetts General Hospital, and [5]Beth Israel Deaconess Medical Center and Department of Medicine, Harvard Medical School, Boston, Massachusetts, USA.

Integrin adhesion molecules mediate lymphocyte migration and homing to normal and inflamed tissues. While the ligand-binding activity of integrins is known to be modulated by conformational changes, little is known about how the appropriate balance of integrin adhesiveness is maintained in order to optimize the migratory capacity of lymphocytes in vivo. In this study we examined the regulation of the gut homing receptor $\alpha_4\beta_7$ integrin by manipulating at the germline level an integrin regulatory domain known as adjacent to metal ion-dependent adhesion site (ADMIDAS). ADMIDAS normally serves to raise the activation threshold of $\alpha_4\beta_7$, thereby stabilizing it in the default nonadhesive state. Lymphocytes from knockin β_7 (D146A) mice, which harbor a disrupted ADMIDAS, not only expressed an $\alpha_4\beta_7$ integrin that persistently adhered to mucosal addressin cell adhesion molecule–1 (MAdCAM-1), but also exhibited perturbed cell migration along MAdCAM-1 substrates resulting from improper de-adhesion of the lymphocyte trailing edge. In vivo, aberrantly activated $\alpha_4\beta_7$ enhanced adhesion to Peyer's patch venules, but suppressed lymphocyte homing to the gut, diminishing the capacity of T cells to induce colitis. Our results underscore the importance of a proper balance in the adhesion and de-adhesion of the $\alpha_4\beta_7$ integrin, both for lymphocyte trafficking to the gut and for colitis progression.

Introduction

Integrin cell adhesion molecules mediate binding to specific ligands in the extracellular matrix and/or on opposing cell surfaces. Integrins are a family of αβ heterodimeric proteins; both α and β subunits have large, structurally complex extracellular domains, a single-pass transmembrane helix, and short cytoplasmic tails (1). The ability of integrins to bind ligands is dynamically regulated by conformational changes. In resting cells, integrins exist predominantly in a nonadhesive state and are converted to an adhesive state upon cellular activation (2). Integrins undergo conformational transitions when the activation of receptor tyrosine kinases or G protein–coupled receptors (GPCRs) leads to the binding of intracellular signaling proteins (e.g., talin) to integrin cytoplasmic domains, thereby triggering conformational signal transmissions to the extracellular domains (3). The integrin extracellular domains undergo structural changes that result in conformations competent for their ligands. This dynamic regulation of integrin adhesiveness has been thought to play an important role in the process of leukocyte migration, in which the appropriate balance between upregulation of ligand binding at the leading edge and downregulation at the trailing edge maintains the forward locomotion of leukocytes (3, 4).

Key structural components within the integrin molecule that stabilize the default nonadhesive state have previously been identified. For example, association of the cytoplasmic tails of the α and β subunits at the membrane-proximal regions is required to maintain the integrin in a nonadhesive state (5). Manipulating the membrane-proximal GFFKR motif of the α subunit cytoplasmic tail leads to the formation of constitutively adhesive integrins, as occurs with the integrins $\alpha_2\beta_1$ (6), $\alpha_L\beta_2$ (5), $\alpha_M\beta_2$ (7), and $\alpha_{IIb}\beta_3$ (8).

The I-like domain of the β subunit ectodomain has a linear cluster of 3 divalent cation-binding sites; the metal ion-dependent adhesion site (MIDAS) is located at the center, with the adjacent to metal ion-dependent adhesion site (ADMIDAS) and ligand-induced metal binding site (LIMBS) at either end (9, 10). Whereas the MIDAS serves to coordinate ligand binding, the ADMIDAS and LIMBS serve to negatively and positively modify ligand binding, respectively. Thus, mutations that disrupt the capacity of ADMIDAS to coordinate cations induce constitutively adhesive states in $\alpha_4\beta_7$ (9) and $\alpha_L\beta_2$ (11), as mutations that perturb the cytoplasmic GFFKR sequence persistently activate integrins.

Loss-of-function strategies including transgenic knockouts and use of function-blocking antibodies have been useful in studying those processes that require the adhesive function of specific integrin receptors (1, 12). However, to understand the importance of dynamic regulation underlying integrin adhesiveness, a unique approach is required; for example, the use of transgenic knockin (KI) mice bearing mutations that alter the regulation of integrin conformations and activity in specific ways. Thus, it has previously been shown that a GFFKR deletion of the α_L subunit from $\alpha_L\beta_2$ constitutively increased cell adhesion to ICAM-1 substrates, resulting in perturbed transendothelial cell migration (13). KI mice that express this constitutively active $\alpha_L\beta_2$ GFFKR deletion exhibited delayed leukocyte migration to inflamed peritoneal cavities (14). This demonstrates that, in at least 1 setting (i.e., constitutively active $\alpha_L\beta_2$ GFFKR deletion), deactivation of the integrin constitutes an important mechanism facilitating cell migration.

Nonstandard abbreviations used: ADMIDAS, adjacent to metal ion-dependent adhesion site; CCL, CC chemokine ligand; CMTMR, 5-(and-6)-(((4-chloromethyl) benzoyl) amino) tetramethylrhodamine; CXCL, CXC chemokine ligand; GPCR, G protein–coupled receptor; HEV, high endothelial venule; IEL, intraepithelial lymphocyte; KI, knockin; LI, large intestine; LPL, lamina propria lymphocyte; MAdCAM-1, mucosal addressin cell adhesion molecule–1; MLN, mesenteric lymph node; PLN, peripheral lymph node; PP, Peyer's patch; PTX, pertussis toxin; RA, retinoic acid; SI, small intestine; SP, spleen.

Conflict of interest: The authors have declared that no conflict of interest exists.

Citation for this article: *J. Clin. Invest.* **117**:2526–2538 (2007). doi:10.1172/JCI31570.

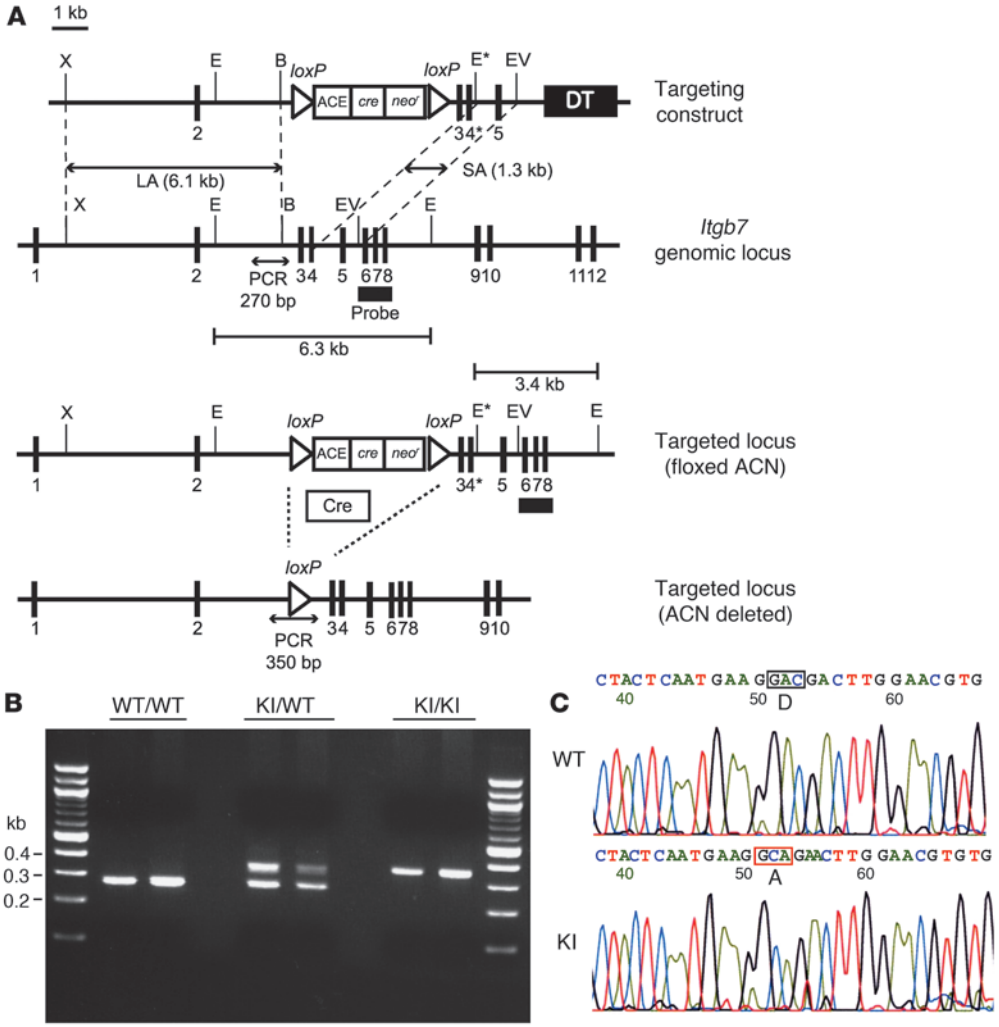

Figure 1

Generation of β_7 (D146A) mice. (**A**) Targeted insertion to the *Itgb7* locus of the floxed ACN cassette, WT exon 3, and the mutated exon 4 (4*) that contains β_7-D146A. The targeting vector, the WT *Itgb7* locus, the targeted *Itgb7* allele containing floxed ACN cassette, and the mutated *Itgb7* (D146A) allele are shown. Exons are shown as filled boxes. Long arm (LA) and short arm (SA) of homology as well as the diphtheria toxin (DT) are also shown. The floxed ACN cassette is deleted in chimeric male mice during spermatogenesis, leaving 1 *loxP* site. An engineered EcoRI site (E*) was designed to identify the targeted allele by Southern blot analysis. X, XhoI; E, EcoRI; B, BglII; EV, EcoRV. The thick black line indicates the probe used to screen for homologous recombinations. (**B**) Genotyping and confirmation of deleted ACN cassette by PCR. Genomic DNA isolated from tails was used for PCR analyses. PCR bands are shown for WT (WT/WT, 270 bp), heterozygote (KI/WT, 350 and 270 bp), and homozygote (KI/KI, 350 bp) samples. (**C**) Sequencing analysis of WT and β_7 (D146A) KI mice. DNA sequencing confirmed an aspartate to alanine substitution at position 146 of the mouse β_7 integrin gene (boxed regions).

Although all integrins are structurally homologous and share large-scale mechanisms for activation (1), many distinctions also exist, in terms of both ligand binding preferences and regulatory interactions with cytoplasmic signaling proteins (15, 16). To obtain a comprehensive understanding of how the regulation of conformational changes contributes to physiological function, it is necessary to first examine both different integrins and different modes of activation. Here, we investigated the physiological consequences stemming from the skewed balance of integrin activation. The $\alpha_4\beta_7$ integrin, via its interaction with mucosal addressin cell adhesion molecule–1 (MAdCAM-1), mediates lymphocyte migration to the gut. In addition, it plays an important role in protective immunity against mucosal pathogens (17–19), as well as in the pathogenesis and progression of gut inflammation (20–22). To skew the balance of $\alpha_4\beta_7$ integrin adhesiveness, we generated KI mice β_7 (D146A), in which the capacity of the ADMIDAS to stabilize the latent I-like domain was disabled. In this way, we demonstrated the critical importance of a proper balance in the adhesion and deadhesion of the $\alpha_4\beta_7$ integrin for both lymphocyte trafficking to the gut and induction of T cell–mediated colitis.

Results

Generation of KI mice bearing the β_7 ADMIDAS mutation. To disable the regulatory function of the ADMIDAS in vivo, we knocked in the point mutation D146A in mouse β_7 corresponding to a previously characterized human β_7 D147A (9). Using a replacement-type gene-targeting strategy (23, 24), we generated a mutant mouse strain with a point mutation in the β_7 gene (*Itgb7*), thereby resulting in replacement of D146 by alanine (Figure 1A). The correct integration of the mutant β_7 gene ($Itgb7^{D146A}$) into the mouse germline was confirmed by PCR and DNA sequencing (Figure 1, B and C). Mice homozygous for the mutant β_7 allele ($Itgb7^{D146A/D146A}$) were designated β_7 (D146A). These mice were born under normal Mendelian ratios, were fertile, and did not exhibit gross abnormalities.

Reduced gut lymphocytes in β_7 (D146A) mice. We analyzed the distribution of lymphocytes in the lymphoid organs of WT and β_7 (D146A) mice. Macroscopic examination showed that the Peyer's patches (PP) of β_7 (D146A) mice (1.7 ± 0.05 mm) were smaller than those of WT mice (2.1 ± 0.04 mm; $P < 0.01$), whereas the spleen (SP), peripheral lymph nodes (PLN), and mesenteric lymph nodes (MLN) were indistinguishable from one mouse strain to the other (data not shown). Although we did not observe gross abnormalities in the villous morphology of the small intestine (SI) (Figure 2A), the number of mononuclear cells including T cells in SI lamina propria

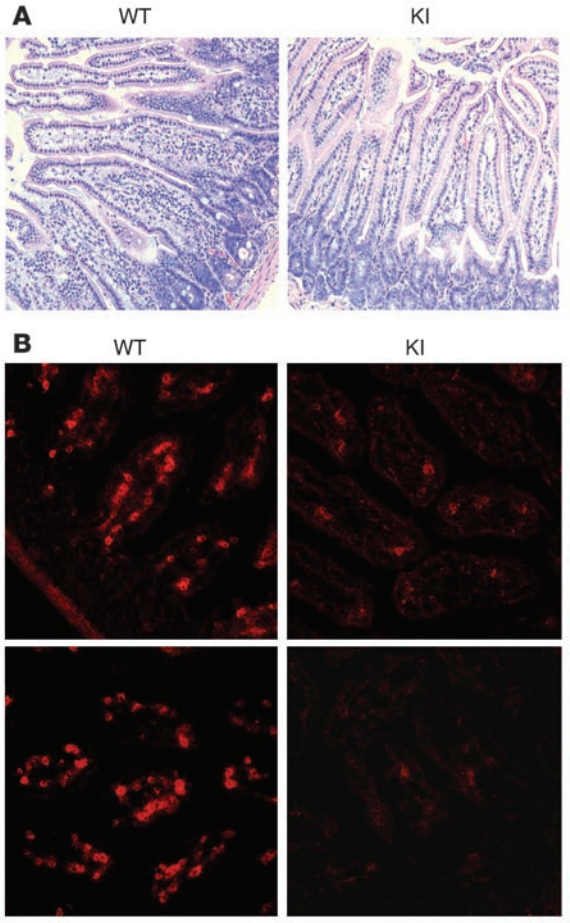

Figure 2
Histology showing reduced T cell numbers in the gut of β_7 (D146A) mice. Representative histology sections (original magnification, ×200) of the SI of WT and β_7 (D146A) KI mice were analyzed by (**A**) hematoxylin and eosin staining and (**B**) immunofluorescent staining with Cy3-conjugated anti-CD3ε mAb.

was greatly reduced (Figure 2, A and B). Flow cytometry analyses showed that compared with WT mice, β_7 (D146A) mice contained significantly fewer lymphocytes in the gut: fewer T cells in PP, fewer intraepithelial lymphocyte (IEL) and lamina propria lymphocyte (LPL) compartments in the SI; and fewer B cells in PP and the large intestine (LI) (Table 1). Because these results suggested the existence of perturbed lymphocyte trafficking to the gut in β_7 (D146A) mice, we investigated the adhesive and migratory behaviors of lymphocytes using the experiments described below. Although the β_7 subunit forms heterodimers with the α_4 and α_E subunits, we focused on $\alpha_4\beta_7$ because it plays the dominant role in lymphocyte homing to the gut (25).

Persistent adhesion to MAdCAM-1 in β_7 (D146A) mononuclear cells. We found that the cell surface expression of β_7 integrins was lower in the lymphocytes from SP of β_7 (D146A) mice compared with that of WT mice (Figure 3A). Whereas decreased expression of α_4 integrins was observed, likely resulting from the reduction in $\alpha_4\beta_7$ expression, the expression of other integrins (e.g., α_L, β_2, and β_1) was not affected. The expression of the activation markers CD62L, CD25, and CD69 proved comparable in WT and β_7 (D146A) lymphocytes (Figure 3B). Similar results were observed in lymphocytes from PLN, MLN, IEL, LPL, and PP (Figure 3A; Supplemental Figure 1; supplemental material available online with this article; doi:10.1172/JCI31570DS1; and data not shown).

Quantitative RT-PCR showed that mRNA expression of the β_7 subunit in WT and β_7 (D146A) splenocytes was similar (Figure 3C). However, immunofluorescent cytometry analyses of permeabilized cells revealed that total expression of the β_7 integrin, including cell surface and intracellular expression, was decreased in β_7 (D146A) cells compared with WT cells (Figure 3D). These results suggested that the stability of the active conformation of the β_7 (D146A) protein might be less than that of WT. Because structurally altered proteins can be destroyed through proteasomal degradation (26), we treated β_7 (D146A) and WT splenocytes with the proteasome inhibitor epoxomicin. Epoxomicin treatment restored the cell surface expression of β_7 (D146A), at least in part, but rarely changed the cell surface expression of the WT β_7 integrin (Figure 3E). In addition, epoxomicin did not affect the expression of WT LFA-1 on β_7 (D146A) and WT cells (Figure 3E). Thus, increased proteasomal degradation of the mutant β_7 (D146A) integrin protein accounts, at least in part, for its reduced cell surface expression. It is worth

Table 1
Distribution of leukocytes

Organ	Mononuclear cells		CD3+		CD19+	
	WT	β_7 (D146A)	WT	β_7 (D146A)	WT	β_7 (D146A)
SP (per mouse)	56.4 ± 4	58.2 ± 2	20.5 ± 2	22.2 ± 2	30 ± 3	30.6 ± 3
Thymus (per mouse)	94.2 ± 8	68.5 ± 17.8	17.3 ± 1.6	12.3 ± 3	ND	ND
PB (per ml)	0.9 ± 0.2	0.7 ± 0.2	0.6 ± 0.1	0.4 ± 0.04	0.3 ± 0.4	0.2 ± 0.1
BM (per 1 femur, 1 tibia)	12.8 ± 1.6	9 ± 1	1.4 ± 0.2	2.1 ± 0.5	8 ± 1.6	5.5 ± 0.2
PLN (per node)	0.9 ± 0.3	1 ± 0.2	0.7 ± 0.2	0.7 ± 0.2	0.2 ± 0.1	0.3 ± 0.1
MLN (per mouse)	5.2 ± 1.5	4.2 ± 0.7	3.4 ± 1.2	2.9 ± 0.4	1.6 ± 0.4	0.7 ± 0.2
PP (per mouse)	1.9 ± 0.2	0.5 ± 0.1[A]	0.4 ± 0.1	0.1 ± 0.03[A]	1.4 ± 0.2	0.4 ± 0.1[A]
SI-IEL (per mouse)	1.3 ± 0.2	0.2 ± 0.03[A]	1.1 ± 0.2	0.1 ± 0.03[A]	ND	ND
SI-LPL (per mouse)	0.8 ± 0.2	0.2 ± 0.04[A]	0.6 ± 0.2	0.1 ± 0.03[A]	0.1 ± 0.03	0.05 ± 0.03
LI (per mouse)[B]	0.4 ± 0.1	0.23 ± 0.04	0.2 ± 0.02	0.2 ± 0.04	0.15 ± 0.03	0.04 ± 0.02[A]

Results (mean ± SEM of at least 5 mice) are presented as cell number × 10^6. [A]$P < 0.05$ versus WT. [B]The cecum was excluded. ND, not detected; PB, peripheral blood.

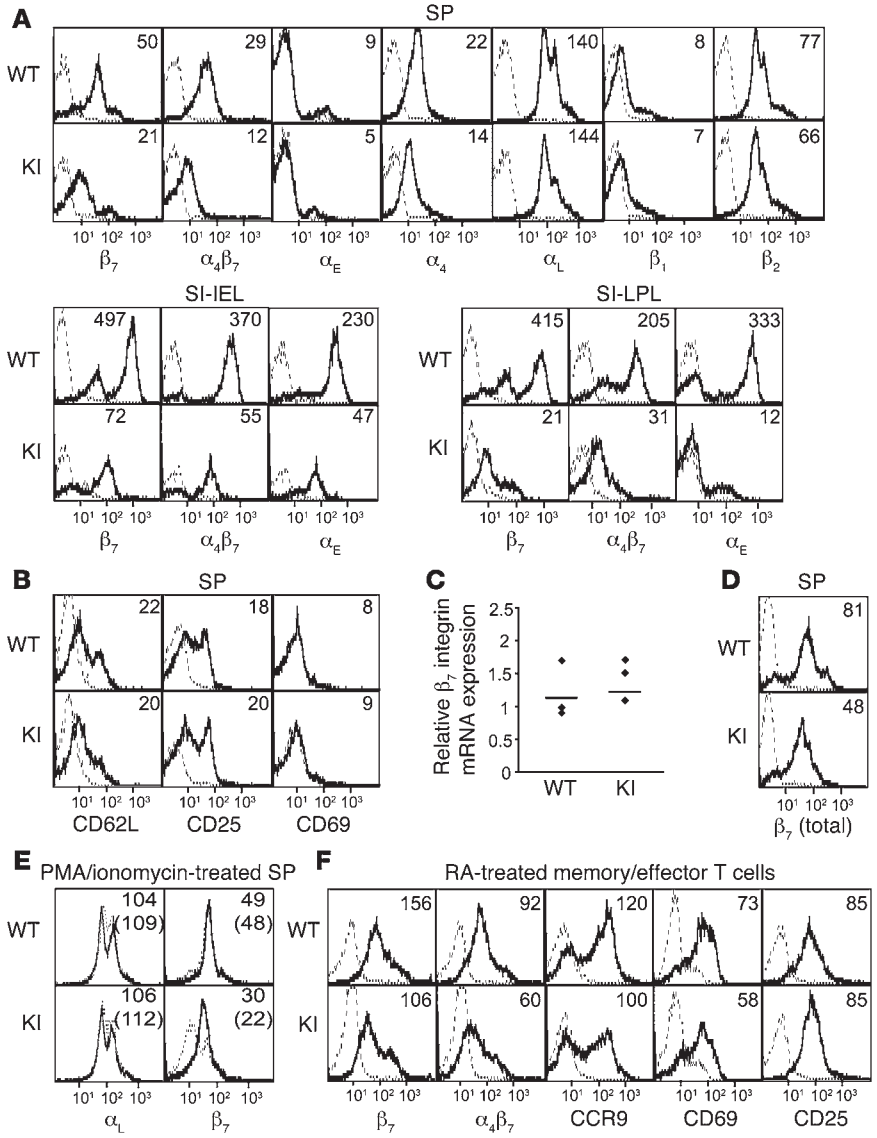

Figure 3
Expression of integrins and activation markers in β_7 (D146A) mice. (**A**) Cell surface expression of integrins on WT and β_7 (D146A) KI lymphocytes from the SP and from SI-IEL and SI-LPL compartments. (**B**) Cell surface expression of activation markers on lymphocytes from SP. (**C**) mRNA expression of β_7 integrins in splenocytes. Real-time quantitative RT-PCR was performed by iCycler (Bio-Rad). The mRNA expression of the β_7 integrin was normalized to that of GAPDH. Dots represent 3 independent data sets; bars denote mean values. (**D**) Total (cell surface plus intracellular) protein expression of β_7 integrins in splenocytes. Total expression was examined by immunofluorescent flow cytometry using permeabilized cells. (**E**) Effects of a proteasome inhibitor on the cell surface expression of integrins. WT and KI splenocytes were treated for 8 hours with epoxomicin (0.5 μM) in the presence of PMA (20 nM) and ionomycin (1 μM). Surface expression of α_L and β_7 integrins was examined by flow cytometry. (**F**) Effects of CD3/CD28/RA treatment on the expression of cell surface receptors. Splenocytes were stimulated with mAbs to CD3 and CD28 for 2 days and treated for 3 days with RA in the absence of mAb stimulation. (**A**, **B**, **D**, and **F**) Numbers denote mean fluorescent intensity (MFI). Binding of isotype control antibodies is shown with dashed lines. (**E**) Numbers denoting MFI values for vehicle-treated (dashed lines) and epoxomicin-treated (solid lines) samples are shown with and without parentheses, respectively.

noting that the reduced cell surface and total expression of integrin LFA-1 was also observed in KI mice that had expressed a constitutively active LFA-1 via a cytoplasmic GFFKR deletion (14).

Despite reduced cell surface expression of $\alpha_4\beta_7$, β_7 (D146A) splenocytes showed enhanced adhesion to MAdCAM-1 substrates (Figure 4A). We analyzed adhesive interaction between $\alpha_4\beta_7$ and MAdCAM-1 substrates under physiological shear stress conditions using a parallel wall flow chamber (9). In the presence of the physiologic cations Ca^{2+} and Mg^{2+} (~1 mM), in which integrins are predominantly maintained in a nonadhesive state, few WT splenocytes interacted with MAdCAM-1. Upon stimulation with Mn^{2+}, which mimics the effects of inside-out signaling and induces high-affinity conformations, WT cells supported shear-resistant firm adhesion. In contrast, β_7 (D146A) splenocytes persistently exhibited firm adhesion to MAdCAM-1 even in the presence of Ca^{2+} plus Mg^{2+} (Figure 4A). Interactions of WT and mutant cells with MAdCAM-1 were abolished by mAb DATK32, confirming that these interactions were mediated by $\alpha_4\beta_7$. Similar results were obtained with lymphocytes from MLN, PLN, and PP (data not shown).

Interaction of $\alpha_4\beta_7$ and MAdCAM-1 is important not only for migration of naive lymphocytes to secondary lymphoid tissues (e.g., PP and MLN), but also for migration of antigen-experienced memory/effector lymphocytes to nonlymphoid tissues (e.g., LPL) (17). We therefore studied the adhesive interactions by memory/effector T cells. To generate in vitro memory/effector T cells with enhanced gut-homing capacity, we stimulated splenocytes with mAbs to CD3 and CD28 for 2 days and treated cells for 3 days with retinoic acid (RA) in the absence of CD3/CD28 stimulation (27). Although this treatment increased $\alpha_4\beta_7$ expression in both WT and β_7 (D146A) T cells, mutant β_7 integrin expression was still lower than that of WT cells (Figure 3F). RA treatment induced comparable levels of upregulated CC chemokine receptor 9 (CCR9), CXCR4, CD69, CD25, and $\alpha_L\beta_2$ integrins in both WT and β_7 (D146A) T cells (Figure 3F and data not shown). RA-treated WT lymphocytes showed a slight increase in basal binding activity to MAdCAM-1 in the presence of Ca^{2+} and Mg^{2+} compared with untreated WT cells (Figure 4B); moreover, a fraction of cells showed firm adhesion. In contrast, a significantly greater number

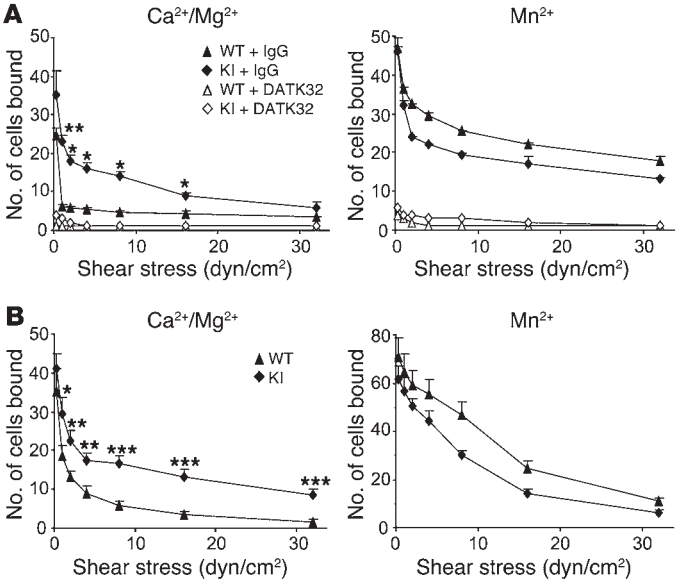

Figure 4
Enhanced adhesive interactions with MAdCAM-1 of β_7 (D146A) cells. Splenocytes (**A**) and RA-treated memory/effector T cells (**B**) from WT and β_7 (D146A) KI mice were infused in 1 mM Mg^{2+}/Ca^{2+} or 1 mM Mn^{2+} into a flow chamber and allowed to accumulate on MAdCAM-1 substrates for 30 seconds at 0.3 dyn/cm^2. Shear stress was incrementally increased from 1 to 32 dyn/cm^2, and adhesive interactions were recorded and analyzed offline. Data are mean ± SEM of 3 independent experiments. *$P < 0.05$, **$P < 0.01$, ***$P < 0.001$ versus WT. In **A**, cells were pretreated with either DATK32 (20 μg/ml) or isotype control IgG (20 μg/ml) for 30 minutes at room temperature.

of RA-treated β_7 (D146A) lymphocytes exhibited firm adhesion over a wide range of shear stresses (1–32 dyn/cm^2; Figure 4B).

Perturbed transendothelial migration of β_7 (D146A) lymphocytes. Because integrins support not only static adhesion but also dynamic cell motility and migration (4), we studied the impact of aberrantly activated β_7 integrins on transmigration and transendothelial migration using a Transwell assay (28). WT and β_7 (D146A) cells transmigrated equally well through an ICAM-1–coated Transwell insert into a CC chemokine ligand 25–containing (CCL25-containing) lower chamber, showing an intact function of $\alpha_L\beta_2$ integrin in β_7 (D146A) cells to mediate transmigration (Figure 5A). In contrast, significantly fewer β_7 (D146A) cells than WT cells transmigrated through a MAdCAM-1–coated insert (Figure 5B). Next, we studied transendothelial migration through a monolayer of a mouse endothelial cell line, bEnd.3, seeded on the insert. We activated bEnd.3 with TNF to upregulate ICAM-1 and MAdCAM-1 expression (29). Compared with WT cells, significantly fewer β_7 (D146A) cells transmigrated through the endothelial monolayer (Figure 5C).

Perturbed migration of β_7 (D146A) lymphocytes on MAdCAM-1 substrates. By directly observing migratory behaviors with live-cell time-lapse video microscopy, we sought to investigate the mechanism(s) by which transendothelial migration of β_7 (D146A) cells was perturbed. We used RA-treated memory T cells from WT and β_7 (D146A) splenocytes. As a control, we first studied cell migration mediated by the interaction of $\alpha_L\beta_2$ with ICAM-1 (Figure 6A, left panels). WT and β_7 (D146A) T cells showed comparable binding to ICAM-1 substrates coimmobilized with CXC chemokine ligand 12 (CXCL12; data not shown). WT and β_7 (D146A) T cells migrated on ICAM-1 at similar velocities [WT, 9.5 ± 0.9 μm/min; β_7 (D146A), 8.8 ± 0.9 μm/min] and showed comparable directional movements as assessed by mean displacement values [WT, 58.2 ± 8.2 μm; β_7 (D146A), 60.5 ± 8.8 μm]. These data confirm that CXCL12-stimulated migration through LFA-1 is not affected by the β_7 ADMIDAS mutation.

On MAdCAM-1 substrates coimmobilized with CXCL12, significantly more β_7 (D146A) cells remained bound to substrates than did WT cells (data not shown). WT cells migrated on MAdCAM-1 as smoothly and efficiently as on the ICAM-1 substrate (Figure 6A and Supplemental Video 1, left panel). In contrast, β_7 (D146A) cells migrated poorly on MAdCAM-1: the migration velocity and directional movement were reduced by approximately 68% and 45%, respectively, compared with WT cells. An examination of β_7 (D146A) cell behavior revealed that the migratory movements of the leading and trailing edges are not well coordinated. The leading edge and the body of the cell continued to exhibit unproductive protrusions that were frustrated by a failure of the trailing edge to detach (Supplemental Video 1, right panel). Similar results were obtained in studies involving migration on MAdCAM-1 substrates coimmobilized with CCL25 (Figure 6A).

Migrating cells were also observed by immunofluorescent confocal microscopy. WT cells migrating on ICAM-1 and MAdCAM-1, as well as β_7 (D146A) cells migrating on ICAM-1, were polarized normally: they displayed a typically hand mirror–like shape, with a flattened leading edge followed by a short tail (Figure 6B). The leading edge was marked by a dense accumulation of F-actin, as shown by phalloidin–Alexa Fluor 488 staining. In contrast, β_7 (D146A) cells migrating on MAdCAM-1 exhibited extremely extended tails highly enriched in β_7 integrin (Figure 6B, arrows). Interestingly,

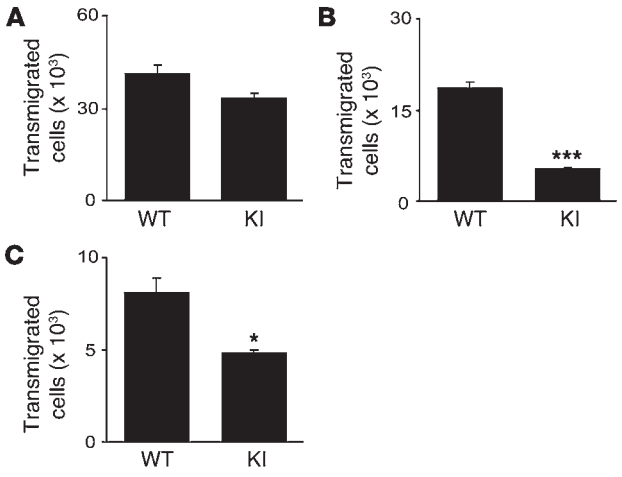

Figure 5
Perturbed transmigration of β_7 (D146A) splenocytes through MAdCAM-1. Transmigration of WT and KI splenocytes toward a CCL25 gradient through ICAM-1–coated (**A**), MAdCAM-1–coated (**B**), and bEnd.3 endothelial monolayer–seeded (**C**) permeable inserts was examined using a modified Boyden chamber assay with a Transwell tissue culture system. Data are mean ± SEM of triplicates from 3 independent experiments. *$P < 0.05$, ***$P < 0.001$ versus WT.

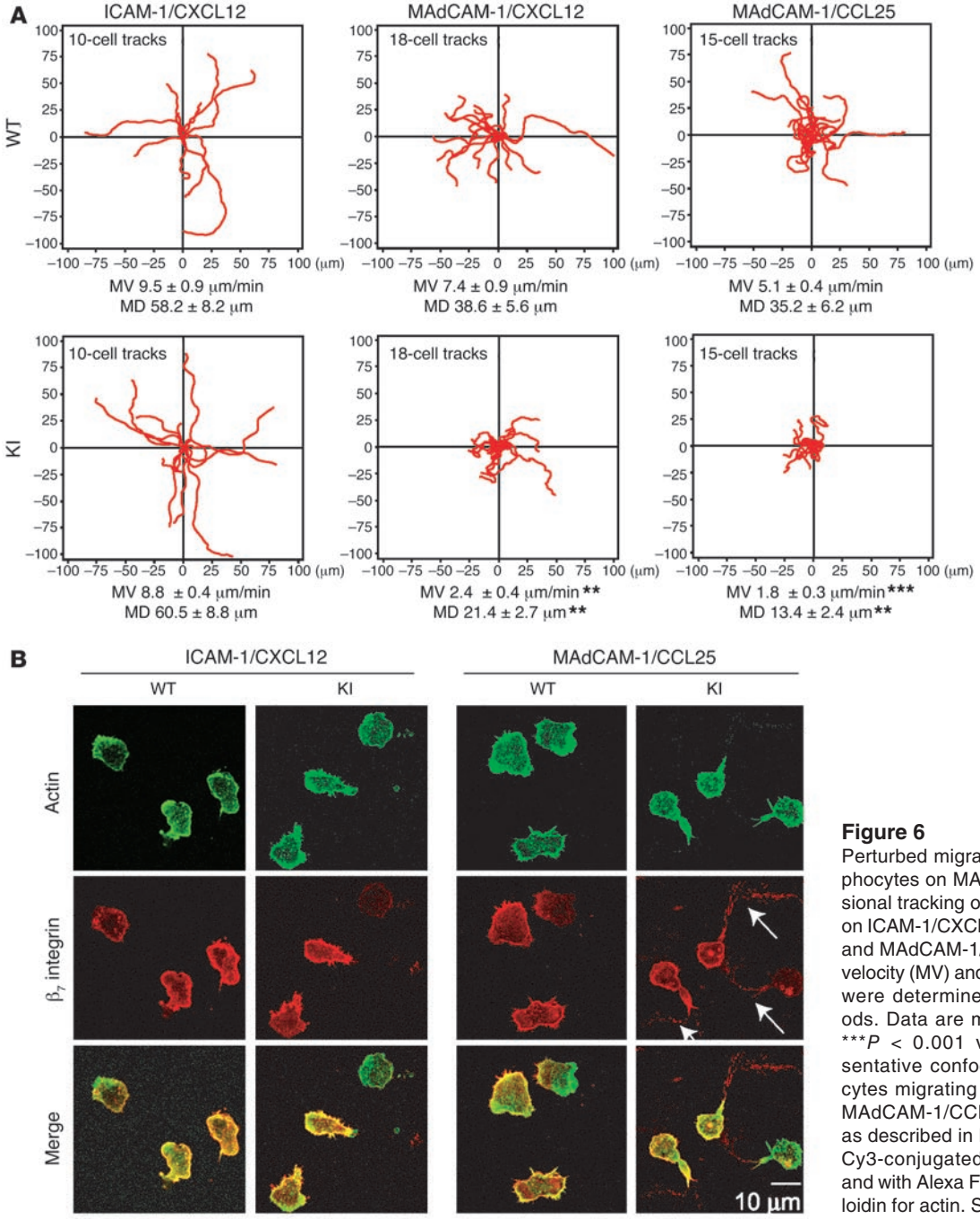

Figure 6
Perturbed migration of β_7 (D146A) T lymphocytes on MAdCAM-1. (**A**) Two-dimensional tracking of T lymphocytes migrating on ICAM-1/CXCL12, MAdCAM-1/CXCL12, and MAdCAM-1/CCL25 substrates. Mean velocity (MV) and mean displacement (MD) were determined as described in Methods. Data are mean ± SEM. $^{**}P < 0.01$, $^{***}P < 0.001$ versus WT. (**B**) Representative confocal images of T lymphocytes migrating on ICAM-1/CXCL12 and MAdCAM-1/CCL25. Samples were fixed as described in Methods and stained with Cy3-conjugated antibody for β_7 integrin and with Alexa Fluor 488–conjugated phalloidin for actin. Scale bar: 10 μm.

the elongated tails lacked F-actin. These results strongly support the idea that decreased migration efficiency of β_7 (D146A) cells on MAdCAM-1–coated substrates (Figure 6) or through the MAdCAM-1–expressing bEnd.3 endothelial monolayers (Figure 5) is attributable to the perturbed detachment of the tail.

Increased firm adhesion of β_7 (D146A) lymphocytes to PP venules in vivo. We next sought to determine how the ADMIDAS β_7 mutation (D146A) affected the adhesive interactions of lymphocytes in vivo. Because rapid chemokine-induced $\alpha_4\beta_7$ integrin binding to MAdCAM-1 in high endothelial venules (HEVs) plays an important role in selective lymphocyte homing to the gut (30, 31), we employed intravital microscopy to study the adhesive interactions of lymphocytes with PP venules. We attempted to correlate the cell surface expression of β_7 integrins by comparing β_7 (D146A) cells with $\beta_7^{+/-}$ cells, which express lower levels of WT β_7 integrins than do WT cells. However, cell surface β_7 integrin expression in $\beta_7^{+/-}$ cells still remained higher than that of β_7 (D146A) cells (Figure 7A).

We injected the same number (2.5×10^7) of calcein-labeled β_7 (D146A) or $\beta_7^{+/-}$ splenocytes into anesthetized WT syngeneic recipient mice that had been prepared for intravital microscopy of PP. The injected cells were then observed and video-recorded entering and interacting with PP venules for 1 hour. Offline analyses of videos showed that comparable numbers of β_7 (D146A) and $\beta_7^{+/-}$ cells were observed entering PP venules [β_7 (D146A), 49.4 ± 5.3

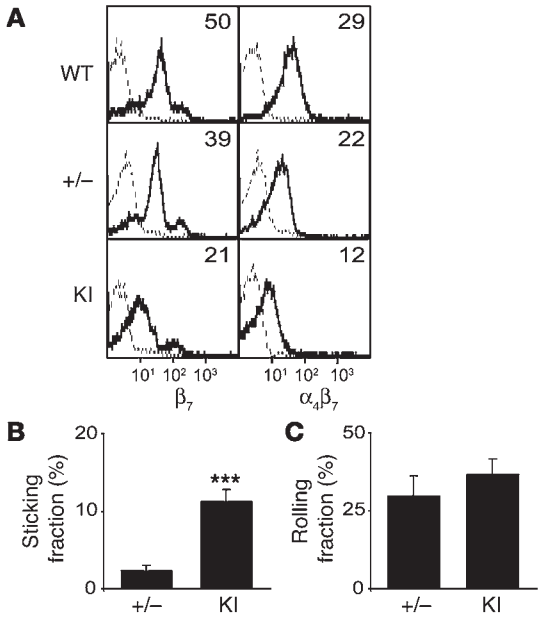

Figure 7
Increased firm adhesion of β_7 (D146A) cells in vivo to PP venules. (**A**) Cell surface expression of β_7 integrins in WT, $\beta_7^{+/-}$ (+/–), and KI lymphocytes. MFI values are shown. Staining with anti-integrin and isotype control mAbs is shown by solid and dashed lines, respectively. (**B** and **C**) Adhesive interactions of $\beta_7^{+/-}$ and KI cells to PP venules studied by intravital microscopy. Fractions of sticking (**B**) and rolling (**C**) cells out of total flowing cells are shown. Data are mean ± SEM of 7 different PP venules analyzed per group in 2 independent experiments. ***$P < 0.001$ versus $\beta_7^{+/-}$.

cells/venule; $\beta_7^{+/-}$, 55.7 ± 10.9 cells/venule]. Whereas similar fractions of cells rolled on PP venules in 2 groups (Figure 7C), significantly more β_7 (D146A) cells made firm adhesions to PP venules than $\beta_7^{+/-}$ cells (Figure 7B). These data demonstrated in vivo the increased adhesiveness of β_7 (D146A) cells to PP venules.

Suppression of β_7 (D146A) lymphocyte migration to the gut. Upregulation of $\alpha_4\beta_7$ integrin adhesiveness is critical for lymphocyte homing to the gut (17). However, the importance of the balance of up- and downregulation of $\alpha_4\beta_7$ in lymphocyte homing remains to be elucidated. Using a competitive homing assay (32), we investigated whether the increased adhesion of β_7 (D146A) lymphocytes to PP venules observed by intravital microscopy causes enhanced homing to the gut. Splenocytes freshly isolated from WT and β_7 (D146A) mice were fluorescently labeled with CFSE and 5-(and-6)-(((4-chloromethyl) benzoyl) amino) tetramethylrhodamine (CMTMR), respectively. Equal numbers of WT and β_7 (D146A) cells were mixed and intravenously administered into C57BL/6J-Thy1.1 or C57BL/6J-Ly5.1 mice. Organs were harvested 18 hours after administration, and the homing indices were then determined (32). Whereas WT and β_7 (D146A) lymphocytes homed equally well to SP, PLN, and MLN, β_7 (D146A) cells homed significantly less well to the gut (including PP, SI, and LI) than did WT cells (Figure 8, A and C). We also performed several homing assay experiments to compare β_7 (D146A) and $\beta_7^{+/-}$ splenocytes, obtaining similar results (Supplemental Figure 2).

Lymphocyte homing requires chemokine activation through GPCR signaling pathways to transform integrins from a nonadhesive to an adhesive state (17). As β_7 (D146A) lymphocytes are persistently adhesive to MAdCAM-1 independent of activation, we examined whether mutant cells could home to the gut in the absence of chemokine activation. Prior to injection in recipient mice, we treated both WT and β_7 (D146A) donor cells with pertussis toxin (PTX), which inhibits GPCR signaling. After PTX treatment, absolute numbers of WT and β_7 (D146A) donors homed to PLN, MLN, PP, and SI, but not to SP, were reduced (Figure 8B). Because similarly reduced levels were observed with PTX-treated WT and β_7 (D146A) cells in PLN, the homing index for PLN was close to 1 (Figure 8, B and D). Homing indices were also near 1 for SP, LI, BM, liver, and lung (Figure 8D). In contrast, in MLN, PP, and SI, PTX-treated β_7 (D146A) lymphocytes homed 2- to 4-fold better than did PTX-treated WT cells (Figure 8, B and D). The homing assay using RA-treated memory/effector T cells also showed similar results (Supplemental Figure 2).

For comparison, we examined the in vivo migratory behavior of β_7 integrin–deficient cells (Figure 8, E and F). Unlike WT, homing of β_7-deficent cells to PP, SI, and LI was severely reduced, while homing to MLN was partially reduced. In PTX-treated cells, unlike β_7 (D146A) cells, β_7-deficient cells migrated less to the gut than did WT cells. Therefore, gut-specific homing of lymphocytes was suppressed by the skewed balance of the $\alpha_4\beta_7$ adhesiveness, reflecting either the aberrant activation in β_7 (D146A) cells or the loss of function in β_7-deficient cells.

Reduced capacity of β_7 (D146A) CD4$^+$CD45RB^{high} T cells to induce colitis. The β_7 integrin–mediated migration of T lymphocytes has previously been implicated in the pathogenesis of intestinal inflammation (20–22). We studied the capacity of β_7 (D146A) T cells to induce intestinal inflammation in a T cell transfer colitis model using *Rag1*$^{-/-}$ recipient mice. In other studies employing this model, CD4$^+$CD45RB^{high} donor T cells predominantly populated and elicited chronic inflammation in the colons of recipient mice (33, 34). *Rag1*$^{-/-}$ mice given 1×10^5 WT CD4$^+$CD45RB^{high} T cells presented clinical symptoms of severe colitis, including the progressive loss of body weight over 8–11 weeks following adoptive transfer (Figure 9A). In contrast, *Rag1*$^{-/-}$ mice given an identical number of β_7 (D146A) CD4$^+$CD45RB^{high} T cells appeared healthy and progressively gained body weight (Figure 9A).

Mice given WT donor T cells showed severe colonic inflammation; specifically massive infiltration of mononuclear cells in colonic LP, disruption of epithelial boundaries, and disappearance of goblet cells (Figure 9B and data not shown). In contrast, mice given β_7 (D146A) donor T cells showed a markedly reduced inflammatory infiltration in colonic tissues and maintained normal colonic mucosa architectures. Whereas WT and β_7 (D146A) donor T cells populated within SP and MLN equally well, significantly fewer β_7 (D146A) T cells than WT cells were present in the colonic lamina propria (Figure 9C).

For comparison, we studied donor T cells from β_7-deficient mice. *Rag1*$^{-/-}$ recipient mice given an identical number of β_7-deficient CD4$^+$CD45RB^{high} T cells (1×10^5) exhibited body weight gain comparable to that of *Rag1*$^{-/-}$ mice given β_7 (D146A) T cells (Figure 9A). Histological analyses showed that the colitis induced by β_7-deficient donor cells was as mild as that induced by β_7 (D146A) donor cells (Figure 9B). Like β_7 (D146A) donor cells, fewer β_7-deficient donor cells populated within the colon compared with WT donor cells. However, comparable numbers of WT, β_7 (D146A), and β_7-deficient donor cells were present in SP and MLN (Figure 9C).

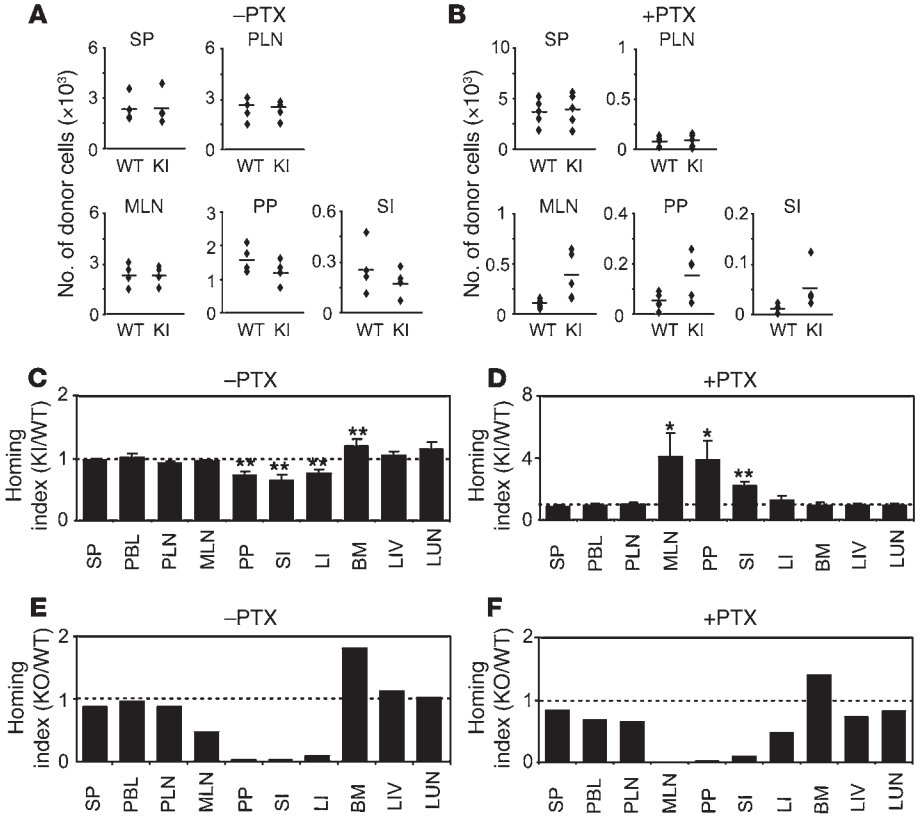

Figure 8
In vivo homing of β_7 (D146A) lymphocytes to the gut is suppressed. Competitive homing assay to compare β_7 (D146A) KI and WT (**A**–**D**) or β_7 KO and WT lymphocytes (**E** and **F**). Equal numbers (2×10^7) of fluorescently labeled cells, either untreated (–PTX; **A**, **C**, and **E**) or treated with PTX (+PTX; **B**, **D**, and **F**), were mixed and injected into C57BL/6J-CD45.1$^+$ congenic mice. The number of homed donor cells (**A** and **B**) and homing indices (**C**–**F**) were determined 18 hours after injection. PBL, peripheral blood lymphocytes; LIV, liver; LUN, lung. Data are mean ± SEM of at least 3 independent experiments. $^*P < 0.05$; $^{**}P < 0.01$ versus SP.

Discussion

An appropriate balance between the nonadhesive and adhesive states of integrins in leukocytes is thought to play an important role in maintaining productive immune responses and avoiding aberrant leukocyte trafficking (14). We studied the impact of a skewed integrin adhesiveness balance on $\alpha_4\beta_7$-mediated lymphocyte homing to the gut. To this end, we disabled the ADMIDAS in the integrin β_7 subunit in the germline by knocking in the β_7-D146A mutation. We have shown that the skewed balance of $\alpha_4\beta_7$ toward a persistently adhesive state perturbed lymphocyte migration on a MAdCAM-1 substrate in vitro. In vivo, the aberrant activation of the β_7 integrin, independent of GPCR signaling, increased firm adhesion to PP venules but did not enhance subsequent homing to the gut. Additionally, in the T cell transfer colitis model using *Rag1*$^{-/-}$ recipient mice, the aberrantly activated β_7 integrin in adoptively transferred donor T cells displayed a reduced capacity to induce inflammation in the colon.

Cell migration is driven by the traction force generated upon adhesive contact; productive and continuous forward movements involve a series of adhesions at the leading edge and de-adhesions at the trailing edge (4). The perturbed migration of β_7 (D146A) cells on MAdCAM-1 substrate as well as through monolayers of a MAdCAM-1–expressing endothelial cell line appears to be attributable to the inability of the trailing edge to de-adhere from MAdCAM-1 substrates. Live-cell imaging of β_7 (D146A) cells migrating on MAdCAM-1 demonstrated "frustrated" lateral migration, in which the leading edge and cell body underwent repeated cycles of forward protrusion, followed by rearward retraction caused by failed detachments of the trailing edge. The β_7 (D146A) cells on MAdCAM-1 exhibited highly polarized and extended trailing edges termed "uropods." Because the extended uropods contained β_7 integrins that remained bound to the substrates, failure to release these integrin-substrate interactions seems to be responsible for such extreme polarization. The lack of F-actin in these uropods suggests that the cytoskeletal linkage between actin and the $\alpha_4\beta_7$ integrin might have been ruptured by overextension, while the bond between aberrantly activated $\alpha_4\beta_7$ and MAdCAM-1 remained intact. An extremely elongated tail was previously observed in monocytes, in which tail retraction was perturbed by interfering with RhoA signaling (35). Moreover, KI lymphocytes that express constitutively active LFA-1 failed to retract the tail during migration on ICAM-1 (14). Thus, the stretched tail appears to be a hallmark of an impaired de-adhesion process.

By mutationally activating integrins, we decoupled the conformational regulation of integrins from those intracellular signaling pathways that impinge on integrin cytoplasmic tails and consequently modify integrin activity. Of note, ligand-bound integrins can transmit signals to the cytoplasm, thereby modifying cytoskeletal protein organization and influencing the migratory velocity of cells, as has been shown in epithelial cell lines (36). Although the role played by ADMIDAS in outside-in signaling remains uncertain, a recent report addressing ADMIDAS in $\alpha_L\beta_2$ suggests that the β_2 ADMIDAS is important for transmitting outside-in signals (11). Although HEK293 T transfectants expressing $\alpha_L\beta_2$ with the ADMIDAS mutation were constitutively adhesive to ICAM-1, they did not express activation-dependent epitopes in the leg domains, nor did they spread or polarize well on ICAM-1 substrate. This finding suggests that conformational signal transmission into the cytoplasm might be perturbed by the β_2 ADMIDAS mutation. In contrast, while we did not directly assess the outside-in signaling

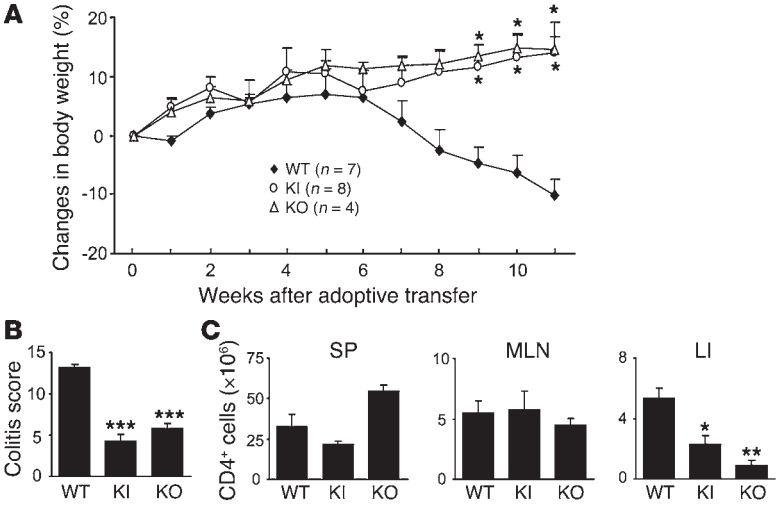

Figure 9

Reduced capacity of β_7 (D146A) T cells to induce colitis. *Rag1*$^{-/-}$ mice were given CD4$^+$CD45RB^{high} T cells (1×10^5) isolated from WT, β_7 (D146A) KI, and β_7 KO splenocytes, and monitored for 11 weeks. (**A**) Body weight changes. Data are mean ± SEM from 2 independent experiments. (**B**) Quantitative histopathologic grading of colitis severity (54). Data are mean ± SEM. (**C**) The numbers of CD4$^+$ T cells in the SP, MLN, and lamina propria of the colon (LI) of recipient mice at week 11 after T cell transfer. Data are mean ± SEM of 4 mice per group. $^*P < 0.05$, $^{**}P < 0.01$, $^{***}P < 0.001$ versus WT cell recipients.

via $\alpha_4\beta_7$ (D146A) in KI cells, β_7 (D146A) lymphocytes were spread across and polarized on MAdCAM-1 substrates as efficiently as did WT cells. This suggests that conformational signal transmission through $\alpha_4\beta_7$ (D146A) can be reserved. Alternatively, it is possible that increased adhesiveness may aberrantly activate signaling though $\alpha_4\beta_7$ (D146A), thereby interfering with optimal regulation of cytoskeletal protein organization during cell migration.

Our data demonstrated that not only upregulation, but also an appropriate balance in up- and downregulation, of integrin $\alpha_4\beta_7$ adhesiveness is important for lymphocytes to efficiently home to the gut. Consistent with in vitro data that β_7 (D146A) cells showed increased cell adhesion to MAdCAM-1 substrates, in vivo observations employing intravital microscopy revealed that more β_7 (D146A) cells firmly adhered to PP venules than did $\beta_7^{+/-}$ cells. However, the increased adhesiveness of β_7 (D146A) cells to the venules did not result in enhanced in vivo homing to the gut. This skewed balance toward the aberrant activation of $\alpha_4\beta_7$ might lead to various consequences, including reduced lymphocyte homing to the gut. However, the most plausible explanation is that the aberrantly activated β_7 integrin in β_7 (D146A) cells perturbs migration over, and transmigration through, HEVs in the gut. This hypothesis is supported our observations of perturbed migration on MAdCAM-1 substrates and suppressed transendothelial migration of β_7 (D146A) cells. Although $\alpha_L\beta_2$ seems to play a dominant role in transendothelial migration (37), impaired de-adhesion of $\alpha_4\beta_7$ from MAdCAM-1 on HEVs could interfere with $\alpha_L\beta_2$-driven diapedesis and migration on and through endothelial cells. Adherent β_7 (D146A) cells that fail to enter gut tissues might eventually become detached from HEVs. This idea is potentially consistent with our data regarding the in vivo kinetics of β_7 (D146A) cells; i.e., compared with WT cells, there were more adherent cells up to 1 hour (as shown by intravital microscopy), but fewer homed cells at 18 hours following adoptive transfer (as shown by a homing assay). While the reduced expression of $\alpha_4\beta_7$ in β_7 (D146A) cells could hinder gut homing, an increased (but not reduced) number of firmly adherent β_7 (D146A) cells to PP venules supports the hypothesis that the aberrant activation of β_7 is the primary mechanism interfering with gut homing. Because β_7 integrins are important for seeding gut-associated lymphoid organs with lymphocytes, the perturbed migration of β_7 (D146A) cells seems to be responsible, at least in part, for smaller PP and reduced numbers of lymphocytes in PP, SI-IEL, SI-LPL, and LI compartments in β_7 (D146A) mice.

Alternatively, it is possible that organs other than the gut that express $\alpha_4\beta_7$ ligands might trap β_7 (D146A) cells, thereby preventing cells from entering HEVs in the gut. The major $\alpha_4\beta_7$ ligand MAdCAM-1 is expressed not only in HEVs, but also in the bone marrow (38) and SP (39). Other than the gut-associated lymphoid tissues, $\alpha_4\beta_7$ can also interact with the VCAM-1 and fibronectin expressed in various tissues (40, 41). Although the default nonadhesive $\alpha_4\beta_7$ prevents WT cells from firmly adhering to ligands outside the gut, aberrant activation of β_7 (D146A) might allow $\alpha_4\beta_7$ to firmly bind to ligands in diverse tissue types. However, intravital microscopy revealed comparable numbers of β_7 (D146A) and $\beta_7^{+/-}$ cells entering PP venules. Competitive homing assay also showed that similar numbers of β_7 (D146A) and WT donor cells stayed in circulation (as shown with peripheral blood lymphocytes; Figure 8). Thus, these data do not necessarily favor the idea that entrapment outside the gut tissues accounts for the reduced homing of β_7 (D146A) cells to the gut.

Upregulation of $\alpha_4\beta_7$-mediated adhesion to MAdCAM-1 by GPCR signaling is required for lymphocyte migration to the gut (30). PTX-treated β_7 (D146A) cells homed better to the gut than did PTX-treated WT cells, supporting the contention that the ADMIDAS mutation induces activation of $\alpha_4\beta_7$ independent of GPCR signaling. However, the mutational activation of $\alpha_4\beta_7$ alone did not fully restore the ability to home to the gut, as PTX-treated β_7 (D146A) cells homed less well to the gut than did untreated β_7 (D146A) cells. Other events regulated by GPCR signaling (e.g., upregulation of $\alpha_L\beta_2$) might be involved in supporting lymphocyte homing to the gut (30).

The ADMIAS mutation is thought to stabilize the open high-affinity conformation of the ligand-binding site in $\alpha_4\beta_7$ (9, 42). It has now become well established that integrin affinity modulation, in response to a range of stimuli (e.g., chemokines), is a central part of its physiologic function (43). For example, Butcher and coworkers have demonstrated that stimulation of GPCRs with chemokines triggers rapid activation of $\alpha_4\beta_7$ in mice that enables lymphocyte arrest on HEV in PP (30, 31). This process is mediated, at least in part, through affinity upregulation (44). Roles for altered or aberrant affinity modulation of integrins in disease have also been demonstrated in a variety of inflammatory diseases.

For example, using conformation-sensitive antibodies that report high-affinity integrins, monocytes from patients with recent episodes of acute myocardial infarction (a pathology associated with excessive monocyte adhesion and migration) were shown to express elevated levels of the high-affinity forms of LFA-1 and Mac-1 (45). Moreover, *Chlamydia pneumoniae* infection (thought to be a key instigator of atherosclerotic disease) of monocytes has been shown to induce their recruitment to the carotid artery in uninfected and nonatherosclerotic mice and to upregulate their adhesion, transendothelial migration, and high-affinity states of LFA-1, Mac-1, and VLA-4 in vitro (46). Finally, polymorphonuclear cells of patients with *Staphylococcus aureus*–induced infection exhibited dramatic upregulation of the high-affinity state of Mac-1 integrin (47). Blocking adhesive interaction of $\alpha_4\beta_7$ by the specific mAb MLN02 was shown to ameliorate ulcerative colitis in a clinical trial (22), supporting the pivotal role of upregulated $\alpha_4\beta_7$ adhesiveness in the pathogenesis and/or progression and maintenance of gut inflammation. Thus, a role for $\alpha_4\beta_7$ affinity modulation for accumulation of lymphocytes into inflamed gut, which has yet to be directly demonstrated, is reasonably supported by those similar observations made for other inflammatory settings as described above (45–47); however, additional roles of valency (i.e., avidity) upregulation are not excluded.

Using a mouse model for inflammatory bowel disease that involves T cell transfer–induced colitis, we studied the impact of aberrantly activated $\alpha_4\beta_7$ in the progression of gut inflammation. Whereas *Rag1*$^{-/-}$ recipients adoptively transferred with WT CD4$^+$CD45RB^{high} donor T cells exhibited severe colitis with a progressive loss in body weight, *Rag1*$^{-/-}$ mice with β_7 (D146A) donor T cells or β_7-deficient donor cells exhibited only minor clinical symptoms and histological findings consistent with colitis. Although similar numbers of WT, β_7 (D146A), and β_7-deficient T cells populated in SP and MLN, significantly fewer β_7 (D146A) and β_7-deficient donor T cells were present in lamina propria of the LI compared with WT donor cells. This is consistent with less severe mucosal inflammation in the colon. In the context of this T cell transfer colitis model, it has been postulated that colitogenic T cells, following adoptive transfer, migrate to secondary lymphoid organs (e.g., MLN), where they proliferate extensively. Activated T cells migrate into the colon where they undergo extensive proliferation and evoke inflammation that further recruits innate immune cells (34). These postmigration events could act to amplify gut inflammation. As β_7 (D146A) and WT donor cells populated in SP and MLN equally well, it is more likely that decreased donor T cell migration to the colon is responsible for reducing colitis in *Rag1*$^{-/-}$ mice given β_7 (D146A) cells. Reduced migration of memory/effector β_7 (D146A) T cells to the gut in a short-time homing assay also supports this possibility. It is noteworthy that the relatively mild defect involving β_7 (D146A) cell migration to the gut could lead to a severe defect: colitis. This might be because perturbation of cell migration by the β_7 ADMIDAS mutation leads to persistent blockade of multiple postmigration events that otherwise amplify and sustain chronic inflammation in the course of colitis progression over the 11-week period. In addition, it is also possible that the proliferation and/or effector activity of β_7 (D146A) donor T cells in vivo in *Rag1*$^{-/-}$ recipient mice might be lower, resulting in a diminished capacity to evoke inflammation in the colon. However, we found that a mixed lymphocyte reaction involving WT and β_7 (D146A) cells was indistinguishable (E.J. Park and M. Shimaoka, unpublished observations).

The data using a germline perturbation of the ADMIDAS in $\alpha_4\beta_7$ shown here, as well as the previous findings regarding the cytoplasmic GFFKR motif in $\alpha_L\beta_2$ (14), both underscore the importance of an appropriate balance of integrin adhesiveness; i.e., activation at the leading edge to form new bonds, followed by deactivation at the trailing edge to allow release and thus forward locomotion. This idea is further supported by the recent finding that a small-molecule agonist to $\alpha_L\beta_2$ suppressed transendothelial migration by preventing uropod detachment (48). Because mutational activation of $\alpha_L\beta_2$ and $\alpha_4\beta_7$ reduced the accumulation of leukocytes in acutely inflamed tissues (14) as well as chronically inflamed tissues as reported in the present study, perturbing de-adhesion of integrins might represent a novel approach for interfering with leukocyte migration to sites of inflammation. In addition, our in vivo data are consistent with the findings by Palecek et al., which showed in in vitro experiments using CHO cells expressing $\alpha_{IIb}\beta_3$ that increased affinity results in maximal migration at a reciprocally lower ligand density (49). The results presented here further enhance the understanding of the concept shown in vitro by Palecek et al. (49) in a complex physiologic process (i.e., tissue-specific homing of lymphocytes) that involves multiple steps (i.e., rolling, firm adhesion, migration, and transmigration) regulated by several mediators and signaling molecules under shear stress.

Methods

Gene targeting. The targeting vector pACN-TV was used, which includes a *loxP*-flanked ACN cassette containing both the *neo*^{r} gene and the *cre*-recombinase gene under the control of the sperm-specific ACE promoter (24). The ACN cassette is deleted in chimeras during spermatogenesis. A 6.1-kb XhoI/BglII fragment containing exon 2 and a 2.2-kb BglII/EcoRV fragment containing exons 3, 4, and 5 were subcloned into the upstream regions and downstream of the *loxP*-flanked ACN cassette, respectively. An engineered EcoRI site was introduced downstream of exon 4 such that a targeted allele from WT was identifiable by Southern blot analysis. D146A was introduced in exon 4 by site-directed mutagenesis. The exonic sequences in the targeting vector were confirmed by DNA sequencing.

The targeting vector was transfected into ES cells of C57BL/6J origin (Bruce-4). G418-resistant ES cell clones were screened for homologous recombination by Southern blot analysis. Homologous integrant ES cell cones were injected into Balb/c blastocytes, and the resulting chimeric males were bred to C57BL/6 females for germline transmission. Offspring were screened for heterozygosity by PCR to confirm a germline transmission and in vivo deletion of the ACN cassette. After intercrossing heterozygotes with each other, the resulting F2 mice were screened to select the homozygote. F5 to F8 generations were used in all experiments.

Mice. C57BL/6J (Charles River Laboratories), Balb/c (Taconic), C57BL/6J-CD90.1 (The Jackson Laboratory), C57BL/6J-CD45.1 (The Jackson Laboratory), β_7 integrin–deficient (The Jackson Laboratory), and Rag-1$^{-/-}$ mice (The Jackson Laboratory) were obtained. All mice were fed a PicoLab Diet 20 (PMI Nutrition) and maintained in a specific pathogen–free animal facility in the Warren Alpert Building at Harvard Medical School. All animal experiments were approved by the Institutional Review Board of the CBR Institute for Biomedical Research.

Antibodies and reagents. The following mAbs were used in this study: CD3ε (145-2C11), CD3 (17A2), CD4 (RM4-5), CD8α (53-6.7), CD19 (1D3), CD28 (37.51), CD18 (C71/16), CD45RB (16A), β_7 (M293), $\alpha_4\beta_7$ (DATK32), CD49d (9C10), CD103 (M290), CD11a (2D7), CD90.1 (OX-7), CD90.2 (53-2.1), MAdCAM-1 (MECA-367), TCR γδ (GL3), and CD16/32 (2.4G2) FcγIII/IIR (BD Biosciences); CD29 (OXM718) (Chemicon International Inc.); β_7 (FIB504) (Santa Cruz Biotechnology Inc.); Cy2-conjugated

anti-rat IgG2a (Jackson ImmunoResearch Laboratories); Cy3-conjugated anti-rat IgG2a (Jackson ImmunoResearch Laboratories); Cy3-conjugated streptavidin (Jackson ImmunoResearch Laboratories); and Phalloidin–Alexa Fluor 488 (Cambrex Biosciences). *All-trans* RA was obtained from Sigma-Aldrich. PTX, phorbol-12-myristate-13-acetate (PMA), and ionomycin were purchased from Calbiochem. The proteasome inhibitor epoxomicin was purchased from Sigma-Aldrich. MAdCAM-1-Fc, CXCL12, and CCL25 were acquired from R&D Systems. Calcein, CFSE, and CMTMR were obtained from Invitrogen.

Cell isolation and flow cytometry. Mononuclear cells were isolated from SP, peripheral blood, PLN, MLN, PP, IEL, LPL, and BM as previously described (50, 51). Multicolor immunofluorescent cytometry was performed as previously described (32, 51) using a FACSCalibur flow cytometer (BD Biosciences). For intracellular staining of integrins, cells were fixed and permeabilized using BD Cytofix/CytopermTM (BD Biosciences) prior to staining with PE-conjugated mAb. Data were analyzed using CellQuest software (BD Biosciences).

Tissue staining. Acetone-fixed cryostat sections (7-μm thickness) were blocked with PBS (pH 7.2), 3% goat serum, and 5% BSA for 30 minute at room temperature. Sections were then incubated for 1 hour with biotinylated mAb to CD3ε (145-2C11) diluted in blocking solution. Bound antibodies were probed with Cy3-conjugated streptavidin. Slides were mounted and images were acquired using a Nikon Eclipse 80i Microscope and SPOT software (Diagnostic Instruments Inc.).

Real-time quantitative RT-PCR. Total RNA from splenocytes was isolated with TRIzol reagent (Invitrogen). A SYBR GreenER Two-Step qRT-PCR Kit was used for first-strand cDNA synthesis and quantitative real-time PCR, and results were quantified with iCycler (Bio-Rad). Sequences for the primer pairs used are as follows: β_7, 5′-CTATCCTCCCTTTCTCTATCAG-3′ (forward) and 5′-GTCTAGGTAGCGCTTGCTTAC-3′ (reverse); GAPDH, 5′-CCAGGTTGTCTCCTGCGACTT-3′ (forward) and 5′-CCTGTTGCTGTAGCCGTATTCA-3′ (reverse). Standard curves were generated, and a threshold was set in the linear part of the amplification curve. Melting curve analysis and agarose gel electrophoresis were performed to assess the purity of the amplified bands.

Epoxomicin treatment. WT and β_7 (D146A) splenocytes were treated for 8 hours at 37°C, 5% CO_2, with the membrane-permeable proteasome inhibitor epoxomicin (0.5 μM) in the presence of PMA (20 nM) and ionomycin (1 μM). Cell surface expression of α_L and β_7 integrins was determined by flow cytometry.

RA treatment of T lymphocytes. Treatment of lymphocytes with RA was done as previously described (27). Briefly, splenocytes were activated for 2 days with immobilized mAbs to CD3 (17A2; 5 μg/ml) and CD28 (37.51; 5 μg/ml) in 10% fetal bovine serum/DMEM (Sigma-Aldrich) in 96-well plates. Activated cells were transferred to mAb-uncoated plates and incubated for 3 days in media containing 200 nM RA (Sigma-Aldrich).

Cell adhesion under shear flow. Cell adhesion under physiologic shear stress was studied as previously described (9). Briefly, a polystyrene Petri dish coated with a 5-mm-diameter, 20-μl spot of 5 μg/ml purified MAdCAM-1–Fc was assembled as the lower wall of a parallel plate flow chamber and mounted on the stage of an inverted phase-contrast microscope (52). Cells were resuspended at 1×10^6/ml in Hank's balanced salt solution, 10 mM HEPES pH7.4, 0.5% BSA containing 1 mM Mg^{2+} and Ca^{2+} or 1 mM Mn^{2+}. Cells were infused in the flow chamber using a syringe pump and allowed to accumulate for 30 seconds at 0.3 dyn/cm^2. Shear stress was then increased every 10 seconds from 1 to 32 dyn/cm^2 in 2-fold increments. The number of cells remaining bound at the end of each 10-second interval was determined. Adhesion of cells was video recorded and analyzed offline.

Transwell assay. Transmigration was studied as described previously (28) with minor modifications, using a modified Boyden chamber assay with a 6.5-mm Transwell tissue culture system (Corning) containing a permeable support insert with 5-μm pore size. In brief, 5×10^4 bEnd.3 mouse brain endothelioma cells (passages 6–10; ATCC) were seeded onto a Transwell insert and cultured to a confluency for 2 days at 37°C and 5% CO_2. The cell monolayers were treated with 5 nM TNF-α (Roche Diagnostics) per well for additional 16 hours to upregulate the expression of ICAM-1 and MAdCAM-1 (29). In some experiments, the inserts were coated with 40 μg/ml of either MAdCAM-1–Fc or ICAM-I–Fc in the place of bEnd.3 cells. WT or KI splenocytes (1×10^6) were added to the upper chamber and allowed to transmigrate for 4 hours to the lower chamber that contained 300 nM CCL25. Transmigrated cells were counted using FACScan flow cytometer (BD Biosciences).

Live-cell migration assay. Cell migration was recorded at 37°C with a culture dish system for live-cell microscopy as previously described (53). Briefly, 20 μg/ml MAdCAM-1–Fc and 2 μM CCL25 or 10 μg/ml ICAM-1–Fc and 10 μg/ml CXCL12-Fc were coated on Delta T chambers (Bioptechs Inc.) at 4°C overnight. After washing with L-15 medium (Cambrex Bioscience), cells were added to the chambers, and differential interference contrast images were acquired using an Axiovert S200 epifluorescence microscope (Zeiss) equipped with a ×63 oil objective coupled to an Orca charge-coupled device camera (Hamamatsu) at 10-second intervals over the course of 25 minutes. Cell migration was analyzed by manually tracing the outline of each cell in 180-second intervals as previously described (48).

Confocal image acquisition and processing. Cells spread on substrates were fixed and stained with mAb β_7 (FIB504) followed by Cy3-conjugated goat-anti-rat IgG2a mAb and Phalloidin–Alexa Fluor 488 for actin. Confocal imaging was conducted on a Radiance 2000 Laser-scanning confocal system (Bio-Rad) using a microscope (model BX50BWI; Olympus) with a ×100 water immersion objective. Imaging processing was performed with OpenLab software.

Intravital microscopy. Intravital microscopy of PP was performed as previously described (30). Briefly, C57BL/6J mice were anesthetized, and the exteriorized bowel segment was positioned for epifluorescence microscopy and video recording of an individual PP on the SI. Calcein-labeled $\beta_7^{+/-}$ or β_7 (D146A) splenocytes (2.5×10^7) were injected through a catheter inserted into the left carotid artery and visualized with a customized intravital microscope (IV-500; Mikron Instruments) equipped with infinity-corrected water-immersion optics (Zeiss). All scenes were recorded on videotape and analyzed offline. The sticking fraction was defined as the percentage of rolling cells that adhered to venules for 30 seconds or more. The rolling fraction was defined as the percentage of total cells passing through the vessel that transiently interacted with PP venules during the observation period.

Competitive in vivo homing assay. A competitive homing assay was conducted as previously described (32). Splenocytes (2×10^7) from β_7 (D146A) or β_7-deficient mice labeled with CFSE were mixed with the same number of WT cells labeled with CMTMR and injected intravenously into C57BL/6J-CD45.1 or C57BL/6J-CD90.1 mice. An aliquot was saved to assess the input ratio (calculated as $[CFSE^+]_{input}/[CMTMR^+]_{input}$). In some experiments, cells were pretreated with 100 ng/ml PTX (EMD Biosciences) at 37°C for 1 hour before labeling. Recipient mice were sacrificed 18 h after injection. The homing index was calculated as the $[CFSE^+]_{tissue}/[CMTMR^+]_{tissue}$ ratio to the input ratio.

T cell transfer colitis. $CD4^+CD45RB^{high}$ naive T cells were isolated from splenocytes using FACSVantage (BD Biosciences) cell sorting with FITC-conjugated anti-CD45RB and PE-conjugated anti-CD4 mAbs. The purity of $CD4^+CD45RB^{high}$ cells was more than 95%. WT, β_7 (D146A), or β_7-deficient $CD4^+CD45RB^{high}$ T cells (1×10^5) in 0.2 ml PBS were injected intraperitoneally into *Rag1*$^{-/-}$ recipient mice. All mice were fed a PicoLab Diet 20 (PMI Nutrition) and maintained in a specific pathogen–free ani-

mal facility at Harvard Medical School. Mice were weighed weekly and observed for signs of illness. At week 11, mice were sacrificed, and histology tissue samples were taken. The degree of colitis was histologically graded as previously described (54).

Statistics. Data are expressed as the mean ± SEM for each group. One-way ANOVA was used for statistical analyses unless otherwise indicated. A P value less than 0.05 was considered significant.

Acknowledgments

We gratefully acknowledge Timothy A. Springer for his valuable advice, Mario R. Capecchi for the self-excision cassette used in pACN-TV, and Klaus Rajewsky for Bruce-4 ES cells. We thank Jieqing Zhu, Azucena Salas, Takashi Nagaishi, Mary Mohrin, and Ronnie Yoo for their technical assistance. This work was supported by NIH grants AI063421 and HL048675 (M. Shimaoka) and AI061663 (U.H. von Andrian), by the Crohn's and Colitis Foundation of America (J.R. Mora), by the American Society of Hematology (M. Shimaoka), and by the Arthritis Foundation (C.V. Carman).

Received for publication January 22, 2007, and accepted in revised form June 26, 2007.

Address correspondence to: Motomu Shimaoka, CBR Institute for Biomedical Research, 200 Longwood Avenue, Room 253, Boston, Massachusetts 02115, USA. Phone: (617) 278-3272; Fax: (617) 278-3232; E-mail: shimaoka@cbrinstitute.org.

1. Hynes, R.O. 2002. Integrins: bi-directional, allosteric, signalling machines. *Cell.* **110**:673–687.
2. Carman, C.V., and Springer, T.A. 2003. Integrin avidity regulation: are changes in affinity and conformation underemphasized? *Curr. Opin. Cell Biol.* **15**:547–556.
3. Kinashi, T. 2005. Intracellular signalling controlling integrin activation in lymphocytes. *Nat. Rev. Immunol.* **5**:546–559.
4. Sanchez-Madrid, F., and del Pozo, M.A. 1999. Leukocyte polarization in cell migration and immune interactions. *EMBO J.* **18**:501–511.
5. Lu, C., and Springer, T.A. 1997. The α subunit cytoplasmic domain regulates the assembly and adhesiveness of integrin lymphocyte function-associated antigen-1 (LFA-1). *J. Immunol.* **159**:268–278.
6. Wang, Z., Leisner, T.M., and Parise, L.V. 2003. Platelet alpha2beta1 integrin activation: contribution of ligand internalization and the alpha2-cytoplasmic domain. *Blood.* **102**:1307–1315.
7. Kanse, S.M., Matz, R.L., Preissner, K.T., and Peter, K. 2004. Promotion of leukocyte adhesion by a novel interaction between vitronectin and the beta2 integrin Mac-1 (alphaMbeta2, CD11b/CD18). *Arterioscler. Thromb. Vasc. Biol.* **24**:2251–2256.
8. O'Toole, T.E., et al. 1994. Integrin cytoplasmic domains mediate inside-out signal transduction. *J. Cell Biol.* **124**:1047–1059.
9. Chen, J.F., Salas, A., and Springer, T.A. 2003. Bistable regulation of integrin adhesiveness by a bipolar metal ion cluster. *Nat. Struct. Biol.* **10**:995–1001.
10. Xiong, J.P., et al. 2002. Crystal structure of the extracellular segment of integrin αVβ3 in complex with an Arg-Gly-Asp ligand. *Science.* **296**:151–155.
11. Chen, J.F., Yang, W., Kim, M., Carman, C.V., and Springer, T.A. 2006. Regulation of outside-in signaling by the β2 I domain of integrin αLβ2. *Proc. Natl. Acad. Sci. U. S. A.* In press.
12. Sheppard, D. 2000. In vivo functions of integrins: lessons from null mutations in mice. *Matrix Biol.* **19**:203–209.
13. Weber, C., Lu, C.-F., Casasnovas, J.M., and Springer, T.A. 1997. Role of $\alpha_4\beta_2$ integrin avidity in transendothelial chemotaxis of mononuclear cells. *J. Immunol.* **159**:3968–3975.
14. Semmrich, M., et al. 2005. Importance of integrin LFA-1 deactivation for the generation of immune responses. *J. Exp. Med.* **201**:1987–1998.
15. Liu, S., Calderwood, D.A., and Ginsberg, M.H. 2000. Integrin cytoplasmic domain-binding proteins. *J. Cell Sci.* **113**:3563–3571.
16. Ginsberg, M.H., Partridge, A., and Shattil, S.J. 2005. Integrin regulation. *Curr. Opin. Cell Biol.* **17**:509–516.
17. Mora, J.R., and von Andrian, U.H. 2006. T-cell homing specificity and plasticity: new concepts and future challenges. *Trends Immunol.* **27**:235–243.
18. Rott, L.S., et al. 1997. Expression of mucosal homing receptor α4β7 by circulating $CD4^+$ cells with memory for intestinal rotavirus. *J. Clin. Invest.* **100**:1204–1208.
19. Artis, D., et al. 2000. Beta7 integrin-deficient mice: delayed leukocyte recruitment and attenuated protective immunity in the small intestine during enteric helminth infection. *Eur. J. Immunol.* **30**:1656–1664.
20. Sydora, B.C., et al. 2002. β7 Integrin expression is not required for the localization of T cells to the intestine and colitis pathogenesis. *Clin. Exp. Immunol.* **129**:35–42.
21. Picarella, D., et al. 1997. Monoclonal antibodies specific for β7 integrin and mucosal addressin cell adhesion molecule-1 (MAdCAM-1) reduce inflammation in the colon of scid mice reconstituted with CD45RBhigh CD4+ T cells. *J. Immunol.* **158**:2099–2106.
22. Feagan, B.G., et al. 2005. Treatment of ulcerative colitis with a humanized antibody to the alpha-4beta7 integrin. *N. Engl. J. Med.* **352**:2499–2507.
23. Kraus, M., et al. 2001. Interference with immunoglobulin (Ig)α immunoreceptor tyrosine-based activation motif (ITAM) phosphorylation modulates or blocks B cell development, depending on the availability of an Igβ cytoplasmic tail. *J. Exp. Med.* **194**:455–469.
24. Bunting, M., Bernstein, K.E., Greer, J.M., Capecchi, M.R., and Thomas, K.R. 1999. Targeting genes for self-excision in the germ line. *Genes Dev.* **13**:1524–1528.
25. Hamann, A., Andrew, D.P., Jablonski-Westrich, D., Holzmann, B., and Butcher, E.C. 1994. Role of α_4-integrins in lymphocyte homing to mucosal tissues in vivo. *J. Immunol.* **152**:3282–3293.
26. Goldberg, A.L. 2003. Protein degradation and protection against misfolded or damaged proteins. *Nature.* **426**:895–899.
27. Iwata, M., et al. 2004. Retinoic acid imprints gut-homing specificity on T cells. *Immunity.* **21**:527–538.
28. Rohnelt, R.K., Hoch, G., Reiss, Y., and Engelhardt, B. 1997. Immunosurveillance modelled in vitro: naive and memory T cells spontaneously migrate across unstimulated microvascular endothelium. *Int. Immunol.* **9**:435–450.
29. Sikorski, E.E., Hallmann, R., Berg, E.L., and Butcher, E.C. 1993. The Peyer's patch high endothelial receptor for lymphocytes, the mucosal vascular addressin, is induced on a murine endothelial cell line by tumor necrosis factor-α and IL-1. *J. Immunol.* **151**:5239–5250.
30. Bargatze, R.F., Jutila, M.A., and Butcher, E.C. 1995. Distinct roles of L-selectin and integrins α4β7 and LFA-1 in lymphocyte homing to Peyer's patch-HEV in situ: the multistep model confirmed and refined. *Immunity.* **3**:99–108.
31. Bargatze, R.F., and Butcher, E.C. 1993. Rapid G protein-regulated activation event involved in lymphocyte binding to high endothelial venules. *J. Exp. Med.* **178**:367–372.
32. Mora, J.R., et al. 2003. Selective imprinting of gut-homing T cells by Peyer's patch dendritic cells. *Nature.* **424**:88–93.
33. Strober, W., Fuss, I.J., and Blumberg, R.S. 2002. The immunology of mucosal models of inflammation. *Annu. Rev. Immunol.* **20**:495–549.
34. Izcue, A., Coombes, J.L., and Powrie, F. 2006. Regulatory T cells suppress systemic and mucosal immune activation to control intestinal inflammation. *Immunol. Rev.* **212**:256–271.
35. Worthylake, R.A., Lemoine, S., Watson, J.M., and Burridge, K. 2001. RhoA is required for monocyte tail retraction during transendothelial migration. *J. Cell Biol.* **154**:147–160.
36. Gupton, S.L., and Waterman-Storer, C.M. 2006. Spatiotemporal feedback between actomyosin and focal-adhesion systems optimizes rapid cell migration. *Cell.* **125**:1361–1374.
37. Carman, C.V., and Springer, T.A. 2004. A transmigratory cup in leukocyte diapedesis both through individual vascular endothelial cells and between them. *J. Cell Biol.* **167**:377–388.
38. Katayama, Y., Hidalgo, A., Peired, A., and Frenette, P.S. 2004. Integrin alpha4beta7 and its counterreceptor MAdCAM-1 contribute to hematopoietic progenitor recruitment into bone marrow following transplantation. *Blood.* **104**:2020–2026.
39. Crowley, M.T., Reilly, C.R., and Lo, D. 1999. Influence of lymphocytes on the presence and organization of dendritic cell subsets in the spleen. *J. Immunol.* **163**:4894–4900.
40. Yang, Y., Cardarelli, P.M., Lehnert, K., Rowland, S., and Krissansen, G.W. 1998. LPAM-1 (integrin alpha 4 beta 7)-ligand binding: overlapping binding sites recognizing VCAM-1, MAdCAM-1 and CS-1 are blocked by fibrinogen, a fibronectin-like polymer and RGD-like cyclic peptides. *Eur. J. Immunol.* **28**:995–1004.
41. Walsh, G.M., Symon, F.A., Lazarovits, A.I., and Wardlaw, A.J. 1996. Integrin $\alpha_4\beta_7$ mediates human eosinophil interaction with MAdCAM-1, VCAM-1 and fibronectin. *Immunology.* **89**:112–119.
42. Xiao, T., Takagi, J., Wang, J.-H., Coller, B.S., and Springer, T.A. 2004. Structural basis for allostery in integrins and binding of ligand-mimetic therapeutics to the platelet receptor for fibrinogen. *Nature.* **432**:59–67.
43. Luo, B.H., Carman, C.V., and Springer, T.A. 2007. Structural basis of integrin regulation and signaling. *Annu. Rev. Immunol.* **25**:619–647.
44. Constantin, G., et al. 2000. Chemokines trigger immediate β2 integrin affinity and mobility changes: differential regulation and roles in lymphocyte arrest under flow. *Immunity.* **13**:759–769.
45. May, A.E., et al. 2002. Urokinase receptor surface expression regulates monocyte adhesion in acute myocardial infarction. *Blood.* **100**:3611–3617.
46. May, A.E., et al. 2003. Recruitment of Chlamydia pneumoniae-infected macrophages to the carotid artery wall in noninfected, nonatherosclerotic mice. *Arterioscler. Thromb. Vasc. Biol.* **23**:789–794.
47. Zimmermann, F., et al. 2005. Expression of elastase on polymorphonuclear neutrophils in vitro and in vivo: identification of CD11b as ligand for the sur-

face-bound elastase. *Shock.* **23**:216–223.
48. Yang, W., et al. 2006. A small molecule agonist of an integrin, alphaLbeta2. *J. Biol. Chem.* **281**:37904–37912.
49. Palecek, S.P., Loftus, J.C., Ginsberg, M.H., Lauffenburger, D.A., and Horwitz, A.F. 1997. Integrin/ligand binding properties govern cell migration speed through cell/substratum adhesiveness. *Nature.* **385**:537–540.
50. Yamamoto, M., Fujihashi, K., Kawabata, K., McGhee, J.R., and Kiyono, H. 1998. A mucosal intranet: intestinal epithelial cells down-regulate intraepithelial, but not peripheral, T lymphocytes. *J. Immunol.* **160**:2188–2196.
51. Park, E.J., et al. 2003. Clonal expansion of double-positive intraepithelial lymphocytes by MHC class I-related chain A expressed in mouse small intestinal epithelium. *J. Immunol.* **171**:4131–4139.
52. Lawrence, M.B., and Springer, T.A. 1991. Leukocytes roll on a selectin at physiologic flow rates: distinction from and prerequisite for adhesion through integrins. *Cell.* **65**:859–873.
53. Dustin, M.L., Carpen, O., and Springer, T.A. 1992. Regulation of locomotion and cell-cell contact area by the LFA-1 and ICAM-1 adhesion receptors. *J. Immunol.* **148**:2654–2663.
54. Neurath, M.F., et al. 2002. The transcription factor T-bet regulates mucosal T cell activation in experimental colitis and Crohn's disease. *J. Exp. Med.* **195**:1129–1143.